Journal of Ceramic Processing Research. Vol. 16, No. 5, pp. 451~456 (2015)

J O U R N A L O F
Ceramic Processing Research

Mechanochemical synthesis and rapid consolidation of nanostructured 2Co-ZrO_2 composite by pulsed current activated heating

Bong-Won Kwak[a], Byung-Su Kim[b] and In-Jin Shon[a,*]

[a]*Division of Advanced Materials Engineering, the Research Center of Hydrogen and Fuel Cell, Chonbuk National University, 664-14 Deokjin-dong 1-ga, Deokjin-gu, Jeonju, Jeonbuk 561-756, Korea*

[b]*Minerals Resources Research Division, Korea Institute of Geoscience and Mineral Resources, Daejeon 305-350 Korea*

Despite of many attractive properties, the low fracture toughness of ZrO_2 ceramic limits its wide application. One of the most obvious tactics to improve the mechanical properties has been to add a reinforcing agent to formulate a nanostructured composite materials. Nanopowders of Co and ZrO_2 were synthesized from 2CoO and Zr by high energy ball milling. The powder sizes of Co and ZrO_2 were about 27 nm and 37 nm, respectively. Dense nanocrystalline 2Co-ZrO_2 composite was consolidated by pulsed current activated sintering method within two minutes from the mechanically synthesized powders(2Co-ZrO_2). The average hardness and fracture toughness values of nanostuctured 2Co-ZrO_2 composite were also investigated.

Key words: Sintering, Composite, Nanomaterial, Mechanical properties, Co-ZrO_2.

Introduction

It is well known that the attractive physical and mechanical properties that can be obtained with metal matrix composites, such as high specific modulus, strength-to weigh ratio, fatigue strength, and temperature stability and wear resistance, have been documented extensively [1-5]. ZrO_2 has a density of 5.98 g cm^{-3}, a Young's modulus of 210 GPa, excellent oxidation resistance and good high-temperature mechanical properties [6, 7]. Co has a density of 8.9 g cm^{-3}, a Young's modulus of 209 GPa and good fracture toughness [7]. Hence, microstructure consisting of Co and ZrO_2 may be able to satisfy the good oxidation resistance and high temperature mechanical properties requirements of successful high temperature structural material.

Traditionally, discontinuously reinforced metal matrix composites have been produced by several processing routes such as powder metallurgy, spray deposition mechanical alloying, various casting techniques and SHS (self-propagating high temperature synthesis). All these techniques are based on the addition of ceramic reinforcements to the matrix materials which may be in molten or powder form. One of all these techniques, high energy ball milling and mechanical alloying of powder mixtures, were reported to be efficient techniques for the preparation of nano-crystalline metals and alloys, which is a combination of mechanical milling and chemical reactions [8].

Nanostructured materials have been widely investigated because they have a wide functional diversity and exhibit enhanced or different properties compared with bulk materials. Particularly, in the case of nanostructured ceramics, the presence of a large fraction of grain boundaries can lead to unusual or better mechanical, electrical, optical, sensing, magnetic, and biomedical properties [9-15]. In recent days, nanocrystalline powders have been developed by co-precipitation, the thermochemical and thermomechanical process named as the spray conversion process (SCP), and high energy milling [16-18]. The sintering temperature of high energy mechanically milled powder is lower than that of unmilled powder due to the increased reactivity, internal and surface energies, and surface area of the milled powder, which contribute to its so-called mechanical activation [19-21]. However, the grain size in sintered materials becomes much larger than that in pre-sintered powders due to rapid grain growth during a conventional sintering process. Therefore, even though the initial particle size is less than 100 nm, the grain size increases rapidly up to 2 μm or larger during conventional sintering [22]. So, controlling grain growth during the sintering process is one of the keys to the commercial success of nanostructured materials. In this regard, the pulsed current activated sintering (PCAS) technique has been shown to be effective in the sintering of nanostructured materials in very short times (within 1 minute) [23-25].

The purpose of this work is to produce nanopowders of Co, ZrO_2 and dense nanocrystalline Co-ZrO_2 composite within two minutes from mechanically synthesized

*Corresponding author:
Tel : +82-63-270-2381
Fax: +82-63-270-2386
E-mail: ijshon@chonbuk.ac.kr

powders (2Co-ZrO_2) using this pulsed current activated sintering method and to evaluate its mechanical properties (hardness and fracture toughness).

Experimental Procedure

Powders of 95% CoO (−325mesh, Alfa) and 99.5 % pure Zr (−325 mesh, Sejong) were used as a starting materials. 2CoO and Zr powder mixtures were first milled in a high-energy ball mill, Pulverisette-5 planetary mill with 250 rpm and for 10 hrs. Tungsten carbide balls (9 mm in diameter) were used in a sealed cylindrical stainless steel vial under argon atmosphere. The weight ratio of ball-to-powder was 30 : 1. Milling resulted in a significant reduction of grain size. The grain sizes of Co and ZrO_2 were calculated by Suryanarayana and Grant Norton's formula [26],

$$B_r(B_{crystalline}+B_{strain})\cos\theta = k\lambda/L + \eta\sin\theta \quad (1)$$

where B_r is the full width at half-maximum (FWHM) of the diffraction peak after instrument correction; $B_{crystalline}$ and B_{strain} are FWHM caused by small grain size and internal stress, respectively; k is constant (with a value of 0.9); λ is wavelength of the X-ray radiation; L and η are grain size and internal strain, respectively; and θ is the Bragg angle. The parameters B and B_r follow Cauchy's form with the relationship: $B = B_r + B_s$, where B and B_s are FWHM of the broadened Bragg peaks and the standard sample's Bragg peaks, respectively.

After milling, the mixed powders were placed in a graphite die (outside diameter, 35 mm; inside diameter, 10 mm; height, 40 mm) and then introduced into the pulsed current activated sintering system made by Eltek in South Korea, shown schematically in Fig. 1. The four major stages in the synthesis are as follows. Stage 1-Evacuation of the system. Stage 2-Application of uniaxial pressure. Stage 3-Heating of sample by pulsed current (on time; 20 μs, off time; 10 μs). Stage 4-Cooling of sample. The process was carried out under a vacuum of 40 mtorr.

The relative densities of the sintered sample measured by the Archimedes method are over 98% of the theoretical value. Microstructural information was obtained from product samples which were polished at room temperature. Compositional and micro structural analyses of the products were made through X-ray diffraction (XRD) and scanning electron microscopy (SEM) with energy dispersive X-ray analysis (EDS). Vickers hardness was measured by performing indentations at load of 20 kg and a dwell time of 15s on the sintered samples.

Results and Discussion

The interaction between 2CoO and Zr, i.e.,

$$2CoO + Zr \rightarrow 2Cu + ZrO_2 \quad (2)$$

is thermodynamically feasible as shown in Fig. 2.

The X-ray diffraction patterns of raw powders and mechanically high energy ball milled powders from raw powders are shown in Fig. 3. In Fig. 3(c), only Co and ZrO_2 was detected. From above results, solid replacement reaction completely occurs during the high energy ball milling. The full width at half-maximum

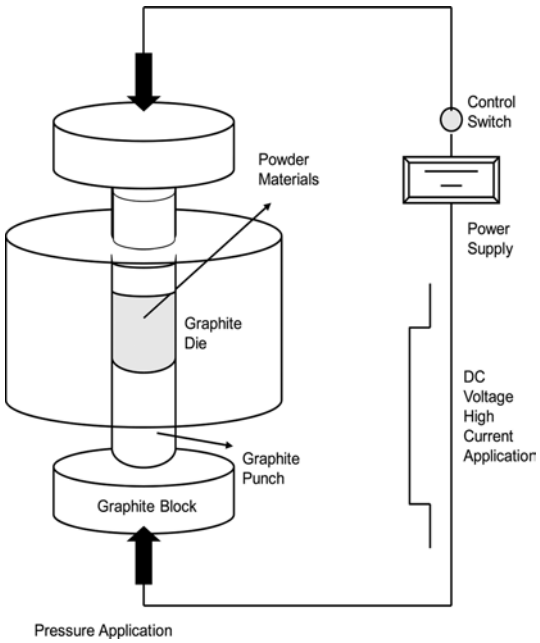

Fig. 1. Schematic diagram of the pulsed current activated sintering apparatus.

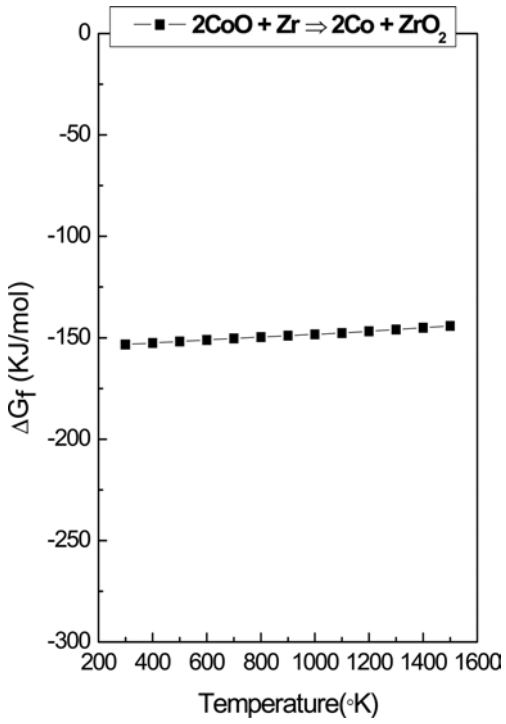

Fig. 2. Temperature dependence of the Gibbs free energy variation by interaction of 2CoO with Zr.

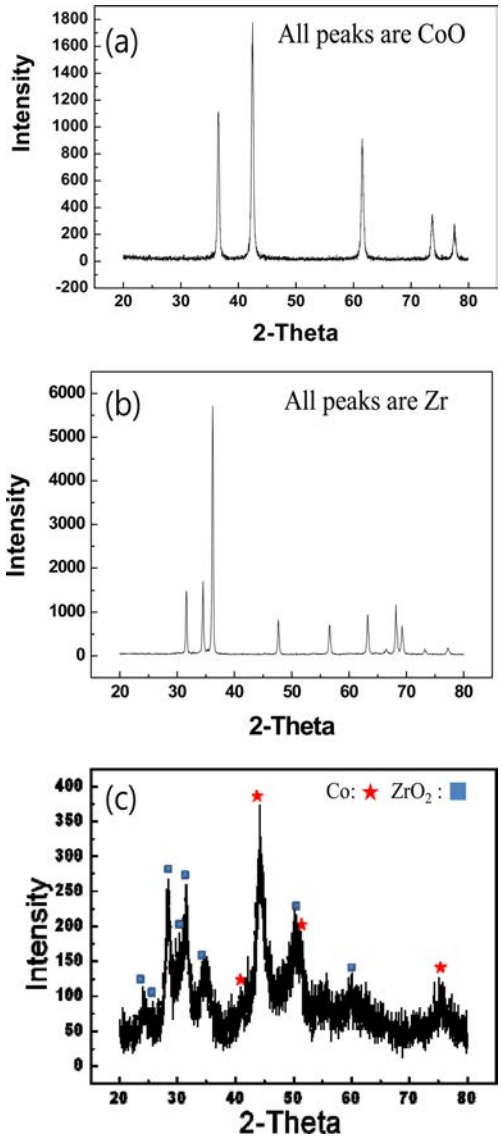

Fig. 3. XRD patterns of raw materials: (a) CoO, (b) Zr, (c) mechanically milled powders.

(FWHM) of the diffraction peak is broad due to refinement of powder and strain. Fig. 4 show plot of Brcosθ versus sinθ to calculate grain size of Cu and ZrO_2. The average grain sizes of ZrO_2 and Co measured by Suryanarayana and Grant Norton's formula were about 37 nm and 27 nm, respectively. FE-SEM and EDS of powders milled for 10 h were shown in Fig. 5. The powders are very fine and have a some agglomeration. The milling process is known to introduce impurities from the ball and/or container. However, in EDS, peaks other than Zr, Co and O were not identified

The shrinkage displacement-time (temperature) curve provides an important information on the consolidation behavior. Fig. 6 shows the shrinkage record of 2Co-ZrO_2 compacts under the applied pressure of 80 MPa. As pulsed current was applied, shrinkage displacement was nearly constant up to heating time of 10 s, and

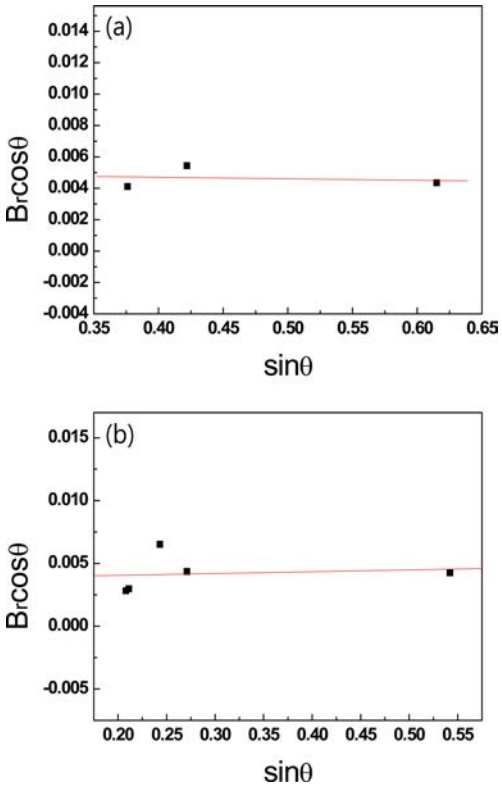

Fig. 4. Plot of $B_r$cosθ versus sinθ for Co(a) and ZrO_2(b) in high energy ball milled powders.

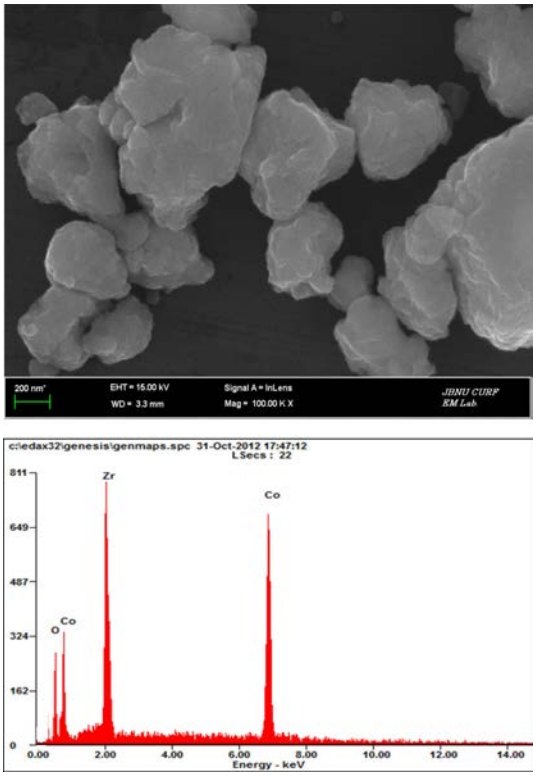

Fig. 5. FE-SEM image and EDS of milled powder.

then abruptly increased above that heating time. Afterwards, they contract almost linearly to 1200 ºC at which the consolidation terminates. The shrinkage

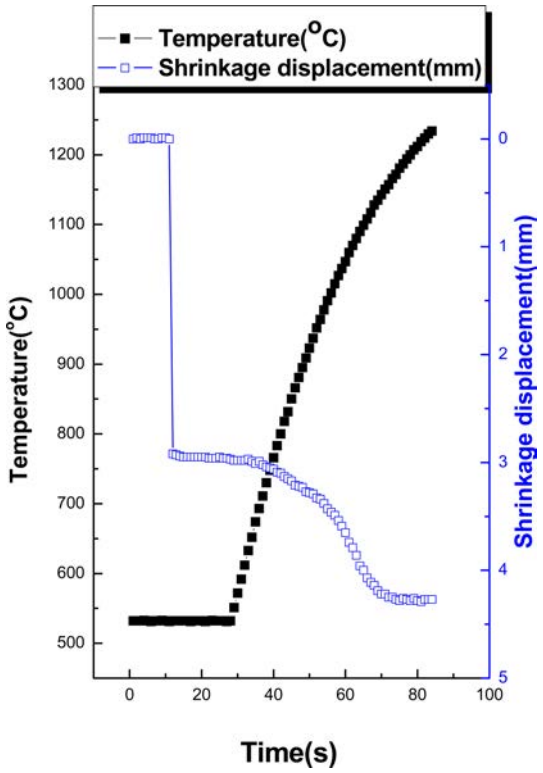

Fig. 6. Variations of temperature and shrinkage displacement with heating time during the sintering of 2Co-ZrO_2 compact by PCAS.

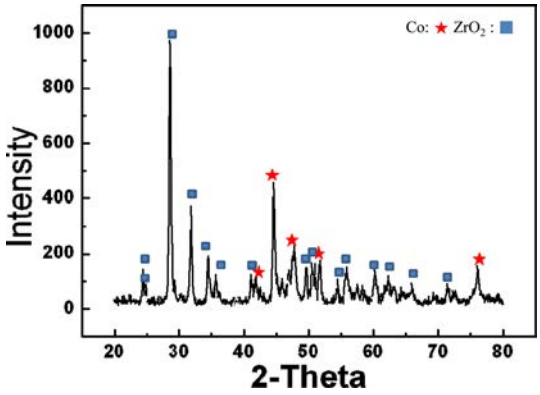

Fig. 7. XRD patterns of 2Co-ZrO_2 composite sintered from high energy ball milled powders.

curve suggests that the consolidation terminates in two minutes. Fig. 7 shows the XRD patterns of 2Co-ZrO_2 composite after sintering. Only Co and ZrO_2 peaks are detected. Again, their particle sizes were calculated by the plot of B_r ($B_{crystalline} + B_{strain}$) cosè versus sinè in Suryanarayana and Grant Norton's formula as shown in Fig. 8. The average grain sizes of Co and ZrO_2 were about 45 and 67 nm, respectively. This means that the grain growth did not greatly occur. FE-SEM images of Co-ZrO_2 composite sintered at 1250 °C from high energy ball milled powders are shown in Fig. 9. The compositesconsists of nanograins. It is considered that the reasons of high density of the nanocomposite obtained within two minutes are as follows. Fistly, raw powders were very fine and many defects were introduced by high-

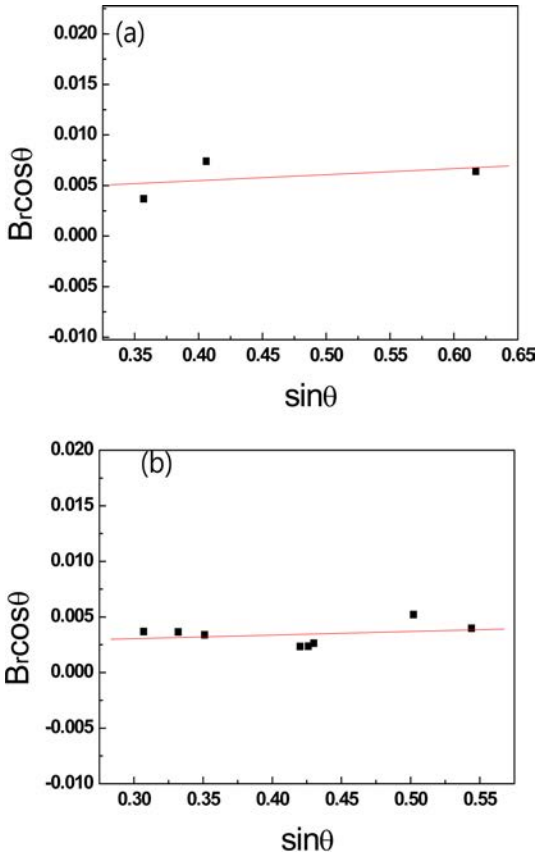

Fig. 8. Plot of $B_r\cos\theta$ versus $\sin\theta$ for Co(a) and ZrO_2(b) in Co-ZrO_2 composite sintered at 1250 °C.

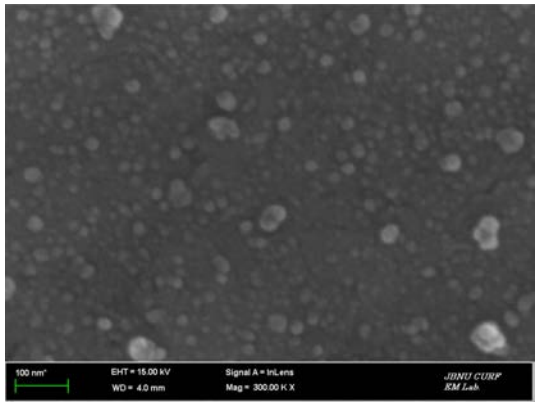

Fig. 9. FE-SEM images of 2Co-ZrO_2 composite sintered from high energy ball milled powders.

energy ball milling. So, the powders were activated, and contact points for diffusion route increased. Secondly, the application of pressure during initial stage sintering adds another term to the surface energy driving force such the total driving force, F_D, is now [27]

$$F_D = \gamma + (P_a r/\pi), \quad (3)$$

where γ is the surface energy, P_a is the applied pressure, and r is the radius of the particle. The effect of pressure on the densification of nanometric, undoped zirconia

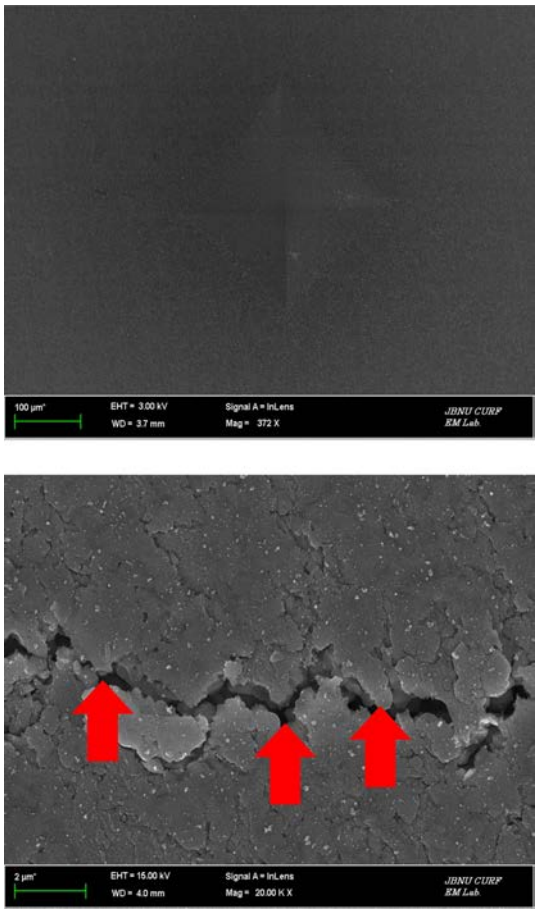

Fig. 10. Vickers hardness indentation and crack propagation in Co-ZrO_2 composite.

during sinter-forging was investigated by Skandan *et al*. [28]. A significant increase in the relative density was observed as the pressure was increased from about 35 to 300 MPa for sintering at 950 ºC for 180 min. Thirdly, The role of the current (resistive or inductive) in sintering and or synthesis has been focus of several attempts aimed at providing an explanation to the observed enhancement of sintering and the improved characteristics of the products. The role played by the current has been variously interpreted, the effect being explained in terms of fast heating rate due to Joule heating, the presence of plasma in pores separating powder particles [29], and the intrinsic contribution of the current to mass transport [30-32].

Vickers hardness measurements were made on polished sections of the 2Co-ZrO_2 composite using a 20 kg_f load and 15 s dwell time. The calculated hardness value of 2Co-ZrO_2 composite sintered 1250 ºC from high energy ball milled powders was 330 kg/mm^2. This value represents an average of five measurements. Indentations with large enough loads produced median cracks around the indent. The length of these cracks permits an estimation of the fracture toughness of the material. From the length of these cracks, fracture toughness values can be determined using by Anstis *et al*. [33] is

$$K_{IC} = 0.016(E/H)^{1/2} \cdot P/C^{3/2} \quad (4)$$

where E is Young's modulus, H the indentation hardness, P the indentation load, and C the trace length of the crack measured from the center of the indentation. The modulus was estimated by the rule mixtures for the 0.67 volume fraction of ZrO_2 and the 0.33 volume fraction of Co using E(ZrO_2) = 210 GPa [6] and E(Co) = 209 Gpa [7]. As in the case of hardness values, the toughness values were derived from the average of five measurements. The toughness value of composite obtained from high energy ball milled are 7 MPa · $m^{1/2}$.

The hardness and fracture toughness of nanostructured ZrO_2 are reported as 690 kg/mm^2 and 3.9 MPa · $m^{1/2}$, respectively [34]. The hardness of 2Co-ZrO_2 composite is lower than that of monolithic ZrO_2 but the fracture toughness is higher than that of ZrO_2 due to addition of ductile Co. Fig. 11 shows indentation and crack propagation in 2Co-ZrO2 composite. In Fig. 10 (b), a crack propagated in a deflective manner (°Ë) in 2Co-ZrO2 composite.

Conclusions

Nanopowders of ZrO_2 and Co were synthesized from Zr and 2CoO by high energy ball milling. The powder sizes of Co and ZrO_2 were 27 nm and 37 nm, respectively. Using the pulsed current activated sintering method, the densification of nanostructured 2Co-ZrO_2 composite was accomplished from mechanically synthesized powders within duration of two minutes. The average grain sizes of Co and ZrO_2 prepared by PCAS were lower than 100 nm, respectively. The average hardness and fracture toughness values obtained from mechanically synthesized powders were 330 kg/mm^2 and 7 MPa · $m^{1/2}$, respectively. The fracture toughness of 2Co-ZrO_2 composite is higher than that of monolithic nanostructured ZrO_2 .

Acknowledgments

This study was supported by a grant in aid awarded by the Basic Research Project of the Korea Institute of Geoscience and Mineral Resources (KIGAM), funded by the Ministry of Science, ICT and Future Planning (GP2015036) and this work was supported by the Human Resources Development program (No.2013 4030200330) of the Korea Institute of Energy Technology Evaluation and Planning (KETEP) grant funded by the Korea government Ministry of Trade, Industry and Energy.

References

1. L. Ceschini, G. Minak, and A.Morri, Composites Science

and Technology 66 (2006) 333-342.
2. S.C. Tjong, and Z.Y. Ma, Materials science and Engineering 29 (2000) 49-113.
3. DJ. Lloyd, Int Mater Rev. 39 (1994) 1-23.
4. 4. JM. Torralba, and F. Velasco, J Mater Process Technol. 133 (2003) 203-205.
5. R. Fan, B. Liu, J. Zhang, J. Bi, and Y. Yin, Mater. Chem. Phys. 91 (2005) 40-46.
6. S. G. Huang, J. the European Ceramic Society 27 (2007) 3269-3275.
7. http://en.wikipedia.org/wiki/Elastic properties of the elements (data page).
8. S. Paris, E.Gaffet, F. Bernard, and Z.A. Munir, Scripta Materialia. 50 (2004) 691-696.
9. J. Karch, R. Birringer, and H. Gleiter, Nature 330, (1987) 556-558.
10. A. M. George, J. Iniguez, and L. Bellaiche, Nature 413 (2001) 54-57.
11. D. Hreniak, and W. Strek, Journal of Alloys and Compounds 341 (2002) 183-186.
12. C. Xu, J. Tamaki, N. Miura, and N. Yamazoe, Sensors and Actuators B: Chemical. 3 (1991) 147-155.
13. D.G. Lamas, A. Caneiro, D. Niebieskikwiat, R.D. Sanchez. D. Garcia, and B. Alascio, Journal of Magnetism and Magnetic Materials 241 (2002) 207-213.
14. Hyun Su Kang, Jung Mann Doh, Jin Kook Yoon, and In Jin Shon, Korean J. Met. Mater. 52 (2014) 759-764.
15. E.S. Ahn, N.J. Gleason, A. Nakahira, and J.Y. Ying, Nano Letters 1 (2001) 149-153.
16. Z. Fang, and J.W. Eason, International Journal of Refractory Metals and Hard Materials 13 (1995) 297-303.
17. A.I.Y. Tok, L. H. Luo, and F.Y.C. Boey, Materials Science and Engineering: A 383 (2004) 229-234.
18. Hyun Su Kang and In Jin Shon, Korean J. Met. Mater. 52 (2014) 623-629.
19. F. Charlot, E. Gaffet, B. Zeghmati, F. Bernard, J. C. Liepce, Mater. Sci. Eng. A262, (1999) 279-288.
20. Geon-Woo Lee, In-Jin Shon, Korean J. Met. Mater. 51 (2013) 95-100.
21. M.K. Beyer, H. Clausen-Schaumann, Chem. Rev. 105 (2005) 2921-2944.
22. J. Jung, S. Kang, Scripta Materialia 56 (2007) 561-564..
23. Na-Ra Park, In-Jin Shon, Journal of Ceramic Processing Research. Vol. 15, No. 2, (2014) 76-81.
24. In-Jin Shon1, Hyoung-Gon Jo, and Hanjung Kwon, Korean J. Met. Mater. 52 (2014) 343-346.
25. In-Jin Shon, Korean J. Met. Mater. 52 (2014) 573-580.
26. C.Suryanarayana, and M.Grant Norton, X-ray Diffraction A Practical Approach, Plenum Press, P.213, New York (1998).
27. R. L. Coble, J. Appl. Phys. 41 (1970) 4798-4807.
28. G. Skandan, H. Hahn, B. H. Kear, M. Roddy and W. R. Cannon, Mater. Lett. 20 (1994) 305-309.
29. Z. Shen, M. Johnsson, Z. Zhao and M. Nygren, J. Am. Ceram. Soc. 85 (2002) 1921-1927.
30. J. E. Garay, U. Anselmi-Tamburini, Z. A. Munir, S. C. Glade and P. Asoka- Kumar, Appl. Phys. Lett. 85 (2004) 573-575.
31. J. R. Friedman, J. E. Garay. U. Intermetallics. 12 (2004) 589-597.
32. J. E. Garay, J. E. Garay. U. Anselmi-Tamburini and Z. A. Munir, Acta Mater., 51 (2003) 4487-4495.
33. G.R. Anstis, P. Chantikul, B.R. Lawn, and D.B. Marshall, J. Am. Ceram. Soc. 64 (1981) 533-538.
34. Seung-Mi Kwak, Hyun-Kuk Park, and In-Jin Shon, Korean J. Met. Mater.Vol. 51, No. 5 (2013) 341-348.